ACS OMEGA

http://pubs.acs.org/journal/acsodf

Article

Graphitic Carbon Nitride-Wrapped Metal-free PoPD-Based Biosensor for Xanthine Detection

Deeksha Thakur, Chandra Mouli Pandey,* and Devendra Kumar*

Cite This: *ACS Omega* 2023, 8, 2328−2336

Read Online

ACCESS | Metrics & More | Article Recommendations | Supporting Information

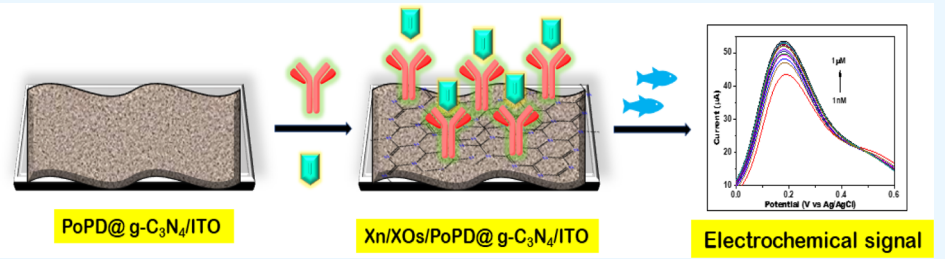

ABSTRACT: A metal-free, enzymatic biosensor was developed using graphitic carbon nitride (g-C_3N_4)-wrapped poly-*ortho*-phenylenediamine (PoPD) for the determination of xanthine (Xn). Field emission scanning electron microscopy, Fourier transform infrared spectroscopy, and X-ray diffraction confirmed the successful formation of the PoPD, g-C_3N_4 nanosheets and PoPD@g-C_3N_4 nanocomposite. Furthermore, the electrochemical behavior of the biosensor was characterized by cyclic voltammetry and electrochemical impedance spectroscopy. The prepared enzyme electrode exhibited maximum response at pH 7.5 with a response time of 5 s, and its sensitivity was 5.798 μAM^{-1}. The nanocomposite shows exceptional sensing capabilities for detecting Xn, having a wide linear range from 1 nM to 1 μM with a relatively low detection limit of 0.001 nM. The biosensor shows good stability (4 weeks) and reproducibility and can detect the presence of Xn from other interfering analytes. Validation of the biosensor with real samples obtained from Rohu (*Labeo rohita*) fish shows that the fabricated biosensor has the requisite potential to be used for Xn detection in meat samples.

1. INTRODUCTION

Graphitic carbon nitride is the most stable allotrope of carbon nitride under ambient conditions. It is a two-dimensional (2D) nanosheet material having a molecular thickness and many attracting physicochemical properties.[1] Among many 2D layered systems, graphitic carbon nitride (g-C_3N_4) is a prominent group of metal-free conjugated polymers with weak van der Waals interactions between layers and a peculiar electrical band structure.[2] Its chemistry of varied morphologies, structures, and applications has received significant interest among researchers. Its exceptional properties, such as its low cost, large surface area, easy preparation, fast electron transfer-conjugation structure, biocompatibility, and catalytic applications, make it an important choice of material for various applications.[3,4] Recently, g-C_3N_4 nanosheets have been used to fabricate biosensors because of their superior catalytic and biocompatibility properties.[5] However, the bare g-C_3N_4 nanosheet synthesized by the thermal condensation procedure has low electrocatalytic activity due to the fast recombination of electrogenerated carriers.[6] A lot of work has been devoted to enhancing the electroactive property of the g-C_3N_4 nanosheet, including nanoscaling, doping, surface modification, and coupling with other conducting polymers.[7] In this context, pairing g-C_3N_4 nanosheets with conducting polymers such as poly-*o*-phenylenediamine (PoPD) is a great way to increase the electrochemical activity of g-C_3N_4.[8]

PoPD is a derivative of polyaniline, having a quinoxaline or 2,3-diaminophenazine repeating unit, which has the advantages of variable conductivity, robust electroactivity, and good optical activity.[9] Its low cost, high stability, and environmental friendliness are crucial for potential applications.[10] PoPD as an interference-rejecting layer offers good selectivity and specificity to the various biomolecules present in biological fluids, which might affect the selectivity of the biosensor.[11] Thus, integrating PoPD with g-C_3N_4 has been considered as an ideal method for increasing electrochemical performance of g-C_3N_4 nanosheets.[8]

Recently, there has been an urgency for quality control in the food industry, increasing demand for fish as a wholesome foodstuff in both developed and developing countries.[12] According to the reported literature, seafood rotting is caused

Received: October 19, 2022
Accepted: December 23, 2022
Published: December 30, 2022

© 2022 The Authors. Published by American Chemical Society

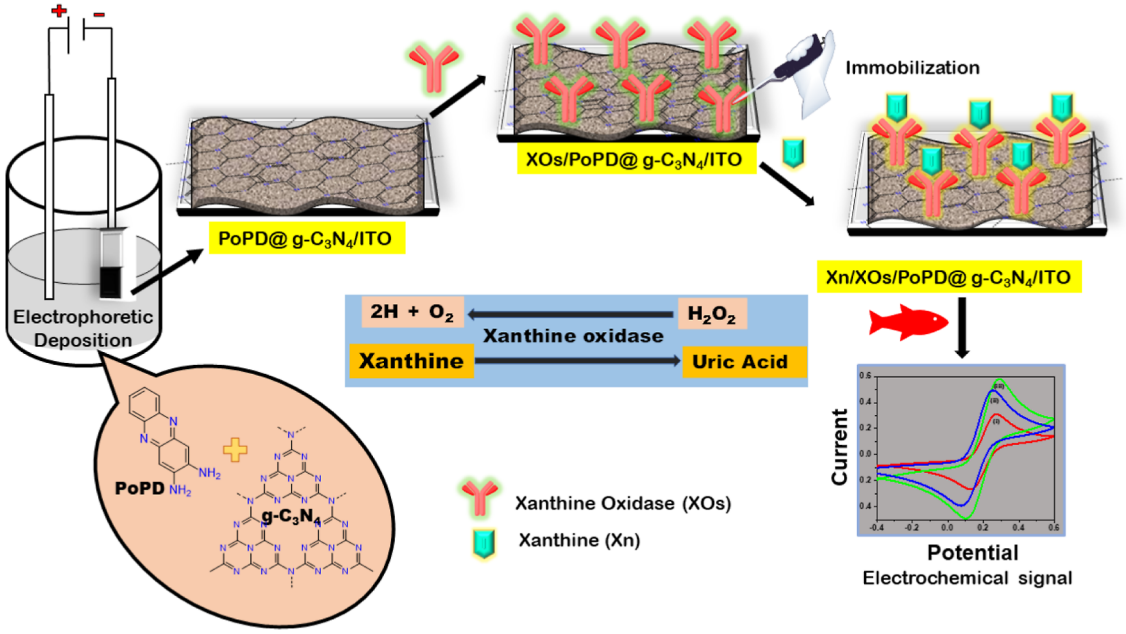

Figure 1. Scheme showing the fabrication of the PoPD@g-C_3N_4 nanohybrid-based biosensor.

by a high concentration of certain enzymes.[13] One of the several enzymes is xanthine (Xn), a key metabolite involved in the disintegration of ATP molecules in fish meat, whose concentration level increases continuously with storage.[14] Since the presence of Xn in fish meat signifies its freshness, the physiological conversion of Xn by xanthine oxidase (XOs) is of great interest.[15] Additionally, measuring the amount of Xn in serum/urine samples makes it possible to gather essential details about specific metabolic disorders such as hyperuricemia, xanthinuria, and renal failure.[16] Numerous analytical methods, such as high-performance liquid chromatography, enzymatic colorimetry, capillary electrophoresis, and so forth, have been used to detect Xn. However, these methods need a lot of effort, resources, and expertise.[17,18] Consequently, there is a critical need to develop a rapid and sensitive method to detect Xn.[19]

Nowadays, electrochemical techniques gained interest as being simple, sensitive, reliable, and affordable to use.[20,21] From the last decade, for hypoxanthine or xanthine detection, various conducting polymer-based nanocomposite biosensors are of interest such as polypyrrole-polyvinyl sulfonate (PPy-PTS) films,[22] polypyrrole-*para*-toluenesulfonate (PPy-pTS),[23] disposable amperometric biosensor with a screen-printed electrode, gold nanoparticles with single-walled carbon nanohorn (GNPs/SWCNH),[24] polymeric mediator/multiwalled carbon nanotube (MWCNT)[25] reduced graphene oxide/iron oxide bio-nanocomposite interface,[26] polymerized 10-[4 *H*-dithieno (3,2-*b*: 2′,3′-*d*) pyrrole-4-yl] decane-1-amine film,[27] and so forth. However, these biosensors show a higher limit of detection, and the linear range may be due to slow electron transfer, poor stability, reusability, fragility, and poor absorption ability, which created requirement for introducing a system with a highly desirable lower detection limit and fast electron transfer. Even, most of the electrochemical biosensors reported for Xn detection usually involve active metal catalysts to provide a higher surface functionality for immobilizing enzymes, increased electroactive surface, and improved charge transfer efficiency.[28]

Herein, efforts have been made to fabricate a metal-free biosensor based on PoPD@g-C_3N_4 nanocomposites, synthesized using a simple oxidative polymerization method. To the best of our knowledge, PoPD@g-C_3N_4 nanocomposite-based biosensors have never been used for Xn detection. With exceptional sensitivity values, it has been revealed that g-C_3N_4 nanosheets modified with P*o*PD for electrode modification can be an effective platform for immobilizing XOs. The synthesized nanocomposite efficiently acted as a metal-free and highly selective sensor to amplify the signal for Xn detection, thus emerging as an innovative electrochemical sensing technique for monitoring fish meat quality.

2. RESULTS AND DISCUSSION

X-ray diffraction (XRD) of P*o*PD (Figure 2A) revealed prominent peaks in the range 2θ = 10−30°, indicating the crystalline behavior of P*o*PD. The broad peak centered at 2θ = 26.5° reveals the polymer chain's local crystallinity.[4]

Furthermore, the crystalline peaks positioned at 2θ = 10.8, 16.5, 18.6, and 28.7° show the nature of the synthesized P*o*PD featuring well-aligned morphology.[29] The XRD diffraction pattern of g-C_3N_4 sheets revealed a weakly intense peak at 2θ = 27.7°, which is indexed to (002) planes.[30] The XRD of g-C_3N_4 and PoPD@g-C_3N_4 showed two similar diffraction peaks at 27.7°, which is attributed to the characteristic (002) plane for interlayer stacking that corresponds to the graphitic structure[31]. It is worth noting that no apparent diffraction peaks of P*o*PD were observed in the PoPD@g-C_3N_4 sample due to the weak crystallinity and small adding content of PoPD.[32]

The FT-IR (Figure 2B) of the g-C_3N_4 nanosheet shows a broad peak at 3164 cm^{-1} for terminal NH_2 or NH groups and C═N stretching peaks at 1575 and 1642 cm^{-1}, stretching peaks at 1245, 1324, and 1404 cm^{-1} were observed for aromatic C−N stretching, and a sharp peak at 808 cm^{-1} is due to the vibration of tri-*s*-triazine units.[4,33] The IR spectrum of the homopolymer PoPD showed the N−H stretching vibration peak at 3143 cm^{-1}, and peaks at 1626 and 1561 cm^{-1} are attributed to the C═C stretching vibrations of quinoid and

https://doi.org/10.1021/acsomega.2c06727
ACS Omega 2023, 8, 2328−2336

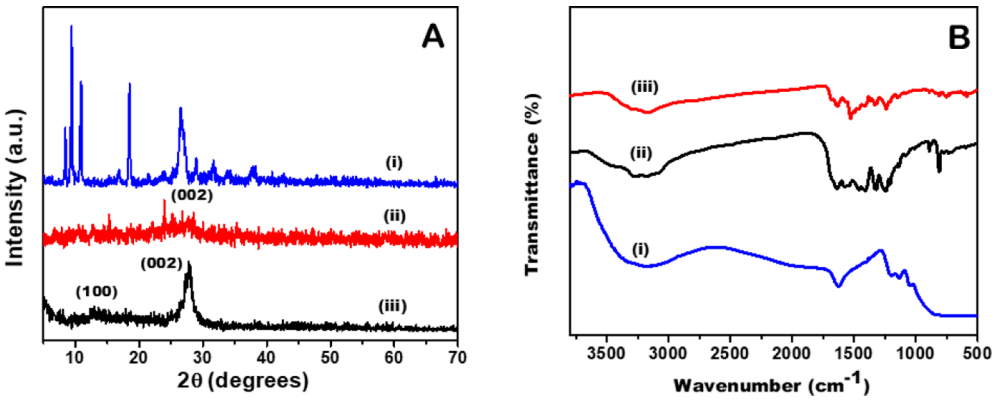

Figure 2. (A) XRD of (i) PoPD, (ii) PoPD@g-C_3N_4 nanohybrid and (iii) g-C_3N_4 nanosheets and (B) FT-IR spectra of (i) PoPD, (ii) g-C_3N_4 nanosheets, and (iii) PoPD@g-C_3N_4 nanohybrid.

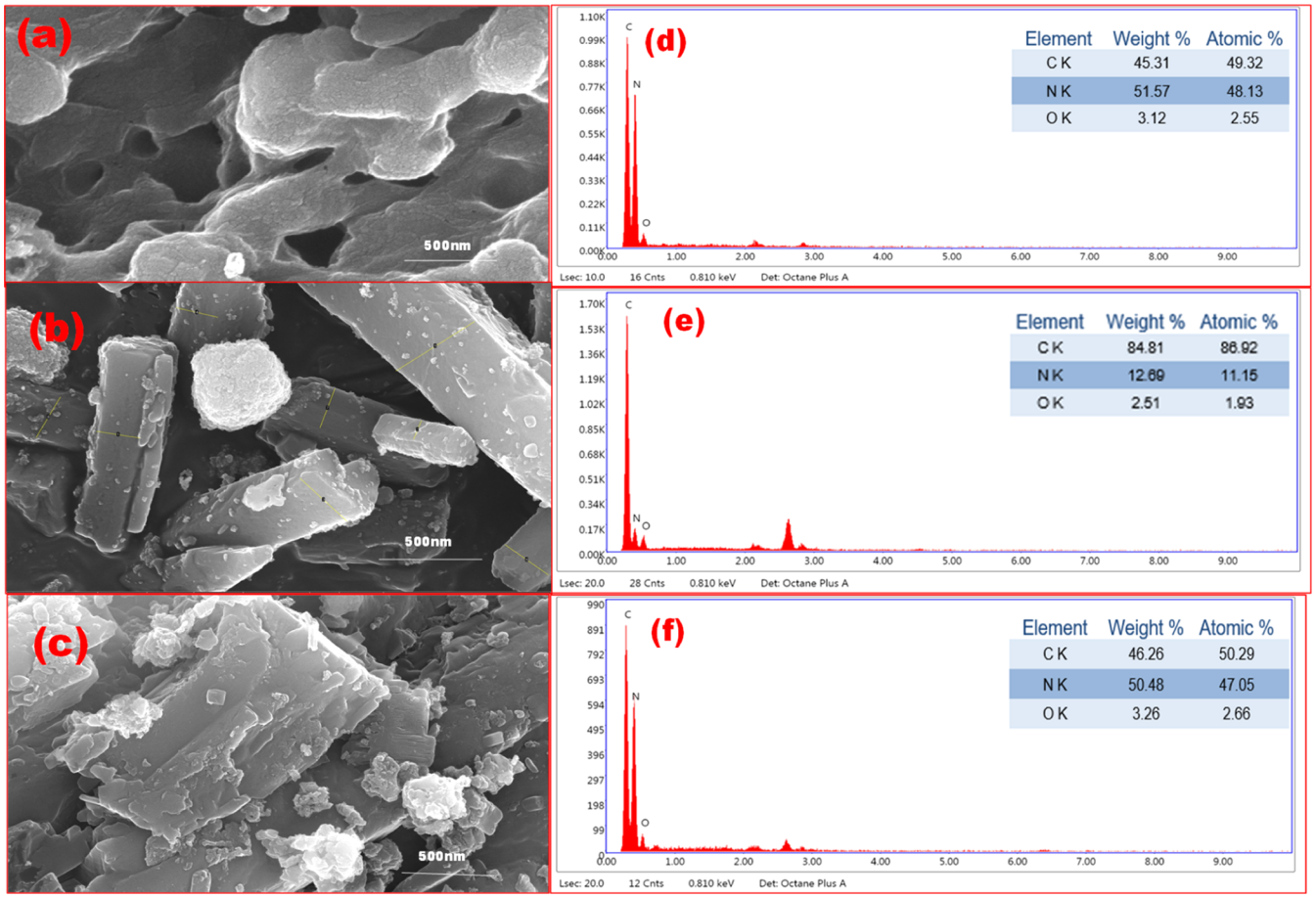

Figure 3. FESEM images (a–c) and EDX images (d–f) for (a) g-C_3N_4, (b) PoPD, and (c) PoPD@g-C_3N_4 nanohybrid obtained at an operating voltage of 15 kV.

benzenoid rings, respectively, while C–N stretching vibrations of quinoid and benzenoid rings appear at 1397 and 1206 cm^{-1}, respectively.[29,34] In the PoPD@g-C_3N_4 nanocomposite, Fourier transform infrared spectroscopy peaks are slightly shifted to higher or lower wavenumber when compared to PoPD. Several characteristic solid peaks in the range of 1700–1200 cm^{-1} are assigned to the stretching vibration of g-C_3N_4. Meanwhile, the characteristic peaks at 820 and 884 cm^{-1} are attributed to the triazine units.[35] Most of the characteristic vibrational peaks of pure g-C_3N_4 are observed in PoPD@g-C_3N_4, indicating the existence of the g-C_3N_4 nanosheet in the composite.

The field emission scanning electron microscopy (FESEM) image of g-C_3N_4 is compared to that of PoPD and PoPD@g-C_3N_4, and the results are shown in Figure 3. As indicated by the microscopic images of g-C_3N_4 (Figure 3a), the layered morphology of g-C_3N_4 and rod-like morphology of PoPD remained the same as in the PoPD@g-C_3N_4 nanocomposite. This confirms that the PoPD particles are randomly distributed on the g-C_3N_4 sheets, which is further evidence for the successful formation of the PoPD@g-C_3N_4 nanocomposite. The EDX spectra shown in Figure 3d–f) confirmed the loading of g-C_3N_4 in the PoPD@g-C_3N_4 framework. In the

https://doi.org/10.1021/acsomega.2c06727
ACS Omega 2023, 8, 2328–2336

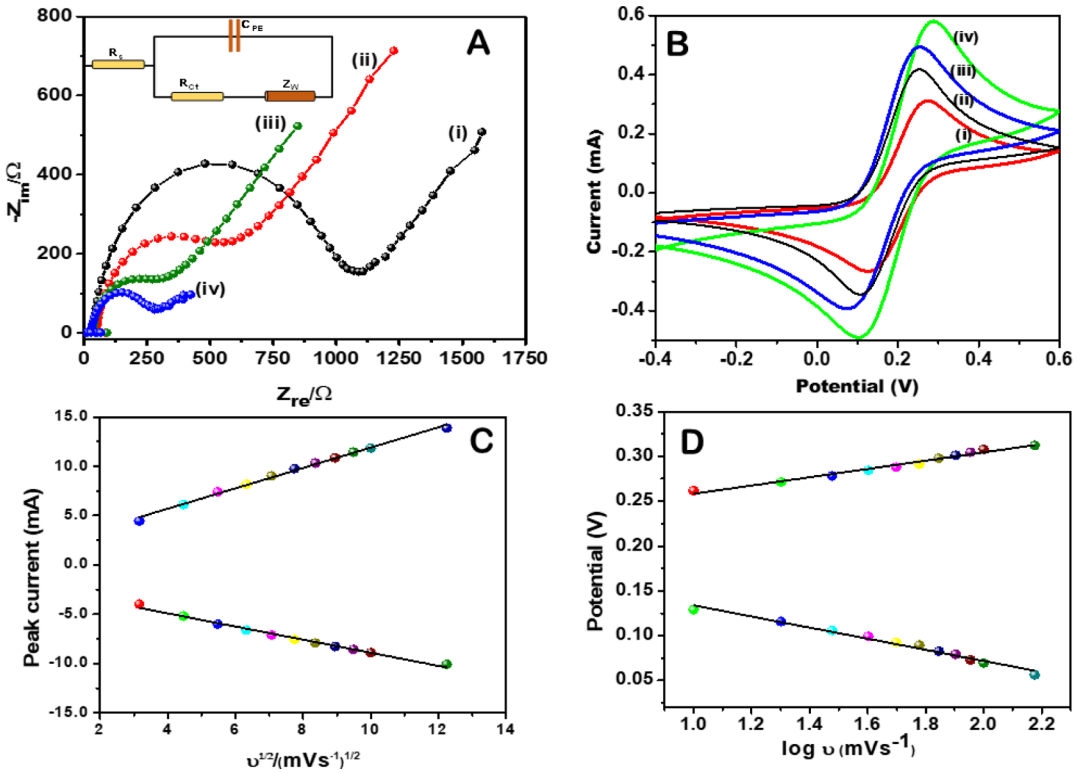

Figure 4. (A) Nyquist diagram for the Faradic impedance for (i) ITO, (ii) g-C_3N_4/ITO electrode, (iii) PoPD/ITO, and (iv) PoPD@g-C_3N_4/ITO electrode measured in PBS solution (pH 7.5) containing 5 mM $[Fe(CN)_6]^{3-/4-}$, in the frequency range from 10^5 to 10^{-2} Hz; (B) CV studies of (i) g-C_3N_4/ITO, (ii) PoPD/ITO, (iii) XOs/PoPD@g-C_3N_4/ITO, and (iv) PoPD@g-C_3N_4/ITO electrodes. The plots of (C) I_{pa}, I_{pc} vs square root of scan rate and (D) potential with the log of scan rate with varying scan rate (10−300 mV) for the PoPD@g-C_3N_4/ITO electrode.

case of PoPD@g-C_3N_4, the wt % of nitrogen content (50.58%) is higher than that of PoPD (12.69%), indicating the successful incorporation of g-C_3N_4 in PoPD. Moreover, the FESEM images, before and after immobilization of XOs on PoPD@g-C_3N_4/ITO with the real image of the fabricated electrode, also validate the morphology change (Figure S6).

2.1. Electrochemical Studies of the Fabricated Electrodes. Electrochemical studies have been carried out for bare ITO, g-C_3N_4/ITO, PoPD/ITO, and PoPD@g-C_3N_4/ITO electrodes using electrochemical impedance spectroscopy (EIS; PBS comprising 5 mM $[Fe(CN)_6]^{3-/4-}$). The Nyquist plot shows a linear region at lower frequencies for the diffusion-controlled electron transfer resistance process and a semicircle region for the electron transfer resistance limited process.[36,37] The solution resistance (R_s), electron transfer resistance (R_{ct}), Warburg impedance (Z_w), and constant phase element (CPE) constitute the equivalent circuit [Figure 4A (inset)]. The obtained Impedance curve has been fitted using FRA software to deduce the different circuit parameters.

The R_{ct} for the ITO electrode was measured to be 1081.5 Ω [curve (i)], whereas the R_{ct} for the g-C_3N_4/ITO, PoPD/ITO, and PoPD@g-C_3N_4/ITO electrodes was found to be 554.43 Ω [curve (ii)], 315.7 Ω [curve (iii)], and 285.08 Ω [curve (iv)], respectively. The significantly smaller diameter of the semicircular Nyquist plot shows a lower electron transfer resistance and a higher interfacial charge transfer characteristic of the PoPD@g-C_3N_4/ITO electrode. The result shows that the addition of PoPD has a favorable impact on the separation and transfer of photogenerated charge carriers, which is compatible with the PoPD@g-C_3N_4 system.[8]

Electrochemical electrode reactions have been studied using electron transfer kinetics based on obtained R_{ct} values. Equations 1 and 2 have been used to compute the apparent electron transfer rate constant (K_{app}) and exchange current per geometric unit area (i_o) for g-C_3N_4/ITO electrodes and PoPD@g-C_3N_4/ITO electrodes.

$$i_o = nRT/R_{ctF} \quad (1)$$

$$K_{app} = RT/n^2F^2AR_{ct}C \quad (2)$$

On comparing, it was found that the PoPD@g-C_3N_4/ITO electrode possesses a higher i_o value (9.007×10^{-5} A cm^{-2}) than g-C_3N_4/ITO (4.631×10^{-5} A cm^{-2}). Furthermore, the values of K_{app} for the g-C_3N_4/ITO and PoPD@g-C_3N_4/ITO electrodes were 0.381×10^{-6} and 0.669×10^{-6} cm s^{-1}, respectively. The increased values of i_o and K_{app} for the PoPD@g-C_3N_4/ITO electrode are due to the synergistic interaction between PoPD and g-C_3N_4 nanosheets, improving conductivity and better electron transfer.

Cyclic voltammetric (CV) studies for g-C_3N_4/ITO, PoPD/ITO, PoPD@g-C_3N_4/ITO, and XOs/PoPD@g-C_3N_4/ITO electrodes in PBS buffer have been shown in Figure 4B. Compared to other electrodes [g-C_3N_4/ITO, 0.31 mA; PoPD/ITO, 0.41 mA; and XOs/PoPD@g-C_3N_4/ITO, 0.49 mA)], the PoPD@g-C_3N_4/ITO electrode displayed a well-defined pair of redox peaks with a greater peak current [curve (iv); 0.58 mA]. The increased peak current of PoPD@g-C_3N_4/ITO suggests that the composite material generated more redox sites for the probe and enhanced electron transport, showing that PoPD and g-C_3N_4 have a positive synergy. After immobilization of the enzyme (XOs) on PoPD@g-C_3N_4/ITO, a well-defined

https://doi.org/10.1021/acsomega.2c06727
ACS Omega 2023, 8, 2328−2336

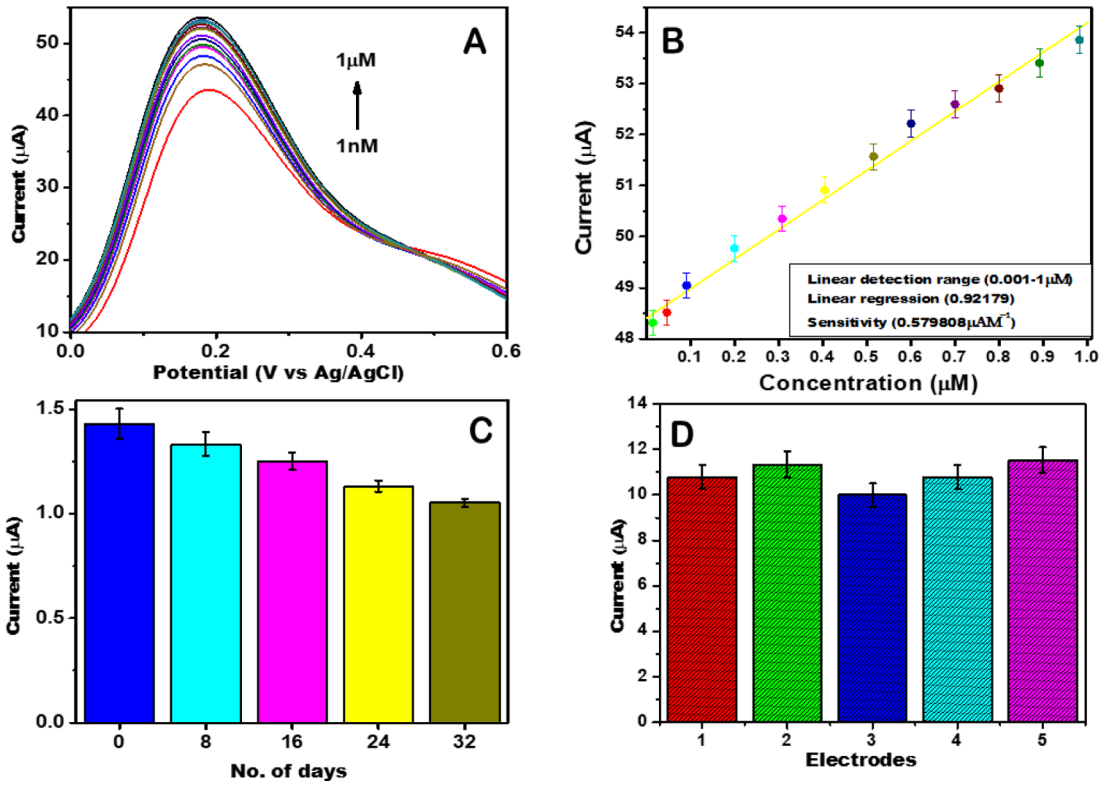

Figure 5. (A) DPV studies showing the response of the XOs/PoPD@g-C_3N_4/ITO electrode with increasing concentration of Xn (0.001−1 μM); (B) calibration plot showing a linear relationship between the magnitudes of current recorded and concentration of Xn; (C) shelf-life tests of the sensor up to 4 weeks, and (D) reproducibility study at five modified electrodes.

redox peak indicates that XOs was successfully immobilized on the surface of the PoPD@g-C_3N_4/ITO and has undergone an oxidation−reduction process at the electrode [curve (iii)].The electroactive surface areas of the electrodes were calculated using the Randles−Sevcik equation

$$I_p = (2.99 \times 10^5)\, \alpha^{1/2}\, n^{3/2} A\, C\, D^{1/2}\, v^{1/2} \quad (3)$$

where n is the number of electrons, v (mV/s) is the scan rate, A (cm^2) is the area of the electrode, C is the concentration in mol/L, D (cm^2/s) is the diffusion coefficient of $[Fe(CN)_6]^{3-/4-}$ in PBS at room temperature which has been reported to be 0.5253×10^{-10} cm^2/s, and I_p (A) is the peak current. The PoPD@g-C_3N_4/ITO exhibits the largest active surface area of 0.997 cm^2 compared to 0.930 and 0.988 cm^2 for g-C_3N_4/ITO and PoPD/ITO, respectively. A high electroactive surface area is expected to offer benefits for electroanalysis.

For the PoPD@g-C_3N_4/ITO (Figure 4C) and XOs/PoPD@g-C_3N_4/ITO (Figure S1) electrodes, the performance of the electrodes was investigated by varying the scan rate (10 to 150 mV/s). It has been observed that the oxidation peak current increases linearly with a positive shift in the peak potential. Both the anodic peak current (I_{pa}) and cathodic peak current (I_{pc}) increase linearly with increasing scan rate and following eqs 3−5, showing surface adsorption-controlled process kinetics for the PoPD@g-C_3N_4/ITO electrode.[38]

$$I_{pa}(\mu A) = 1.5 \times 10^{-3} + 1.0 \times 10^{-3}\sqrt{v}\ (\text{mV/s}) \qquad R = 0.9973 \quad (4)$$

$$I_{pc}(\mu A) = -2.25 \times 10^{-3} - 6.653 \times 10^{-4}\sqrt{v}\ (\text{mV/s}) \qquad R = 0.9941 \quad (5)$$

The anodic and cathodic peak potentials (E_{pa} and E_{pc}) also showed a linear relation with the natural logarithm of scan rate (ln v). The corresponding linear regression equations, eqs 6 and 7, have been given in Figure 4D.

$$E_{pa}(V) = 0.21209 \ln(v) + 0.0462;\ R = 0.9896 \quad (6)$$

$$E_{pc}(V) = 0.19583 \ln(v) - 0.0619;\ R = 0.9903 \quad (7)$$

Using Laviron's equation,[39] the charge transfer coefficient (α) and heterogeneous electron transfer coefficient (K_s) for the PoPD@g-C_3N_4/ITO electrode have been calculated, and they are found to be 0.9105 and 2.3859 s^{-1}, respectively, at a scan rate (v) of 50 mV/s.

The effect of the loading volume of XOs (5 to 30 μL) on the response current toward Xn (0.1 μL) has been shown in Figure S2. The peak current increased initially, up to 20 μL and then reduced with further increasing the loading volume of XOs. An excessive amount of XOs would slow down the passage of electrons, decreasing the sensor's sensitivity. Therefore, 20 μL of XOs solution was used for subsequent studies.

Figure S3 shows the performance of the Xn/XOs/PoPD@g-C_3N_4/ITO electrode in various pH electrolytic solutions ranging from 6.5 to 8.5. Notably, the maximum current response was recorded at a pH of 7.5 in PBS buffer containing 5 mM $Fe[CN_6]^{3-/4-}$. Therefore, pH 7.5 has been chosen as the ideal pH for the electrochemical detection of Xn.

https://doi.org/10.1021/acsomega.2c06727
ACS Omega 2023, 8, 2328−2336

Table 1. Comparison of the Performance of PoPD@g-C_3N_4/ITO With Other CP-Based Biosensors for Xn Detection[a]

S. no.	immobilization matrix	detection technique	linear range (μM)	LOD	ref.
1.	Au-XOR/fMWCNT-PEDOT/GCE	DPV	0.1−10	5.45×10^{-2} μM	40
2.	XODNPs/Au	CV	0.01−1	0.01 μM	41
3.	XO/Poly(l-Asp)/MWCNT/GCE	DPV	0.001−0.004	3.5×10^{-4} μM	42
4.	XOD/ZnO/Ch/c-MWCNT/PANI/Pt	CV	0.1−100	0.1 μM	43
5.	Au-PPy	CV	0.4−100	0.4 μM	44
6.	XOD/c-MWCNT/PANI/Pt	CV	0.6−58	0.6 μM	14
7.	Ch/PPy/AuNPs/GCE	CV	1−200	0.25 μM	45
8.	PANI@TiO_2/ITO	DPV	1−100	0.1 μM	21
9.	poly-TTCA/Au	CV	5−0.001	1 μM	46
10.	PoPD@g-C_3N_4	DPV	0.001−1	0.001 nM	**present work**

[a]Abbreviations: Au: gold nanoparticles; XOR: xanthine oxidoreductase; fMWCNT: functionalized multiwalled carbon nanotube; PEDOT: poly(3,4-ethylenedioxythiophene); GCE: glassy carbon electrode; XODNPs: xanthine oxidase nanoparticle; [poly(l-asp):poly(l-aspartic acid)]; ZnO: zinc oxide; Ch: chitosan; PANI: polyaniline; Pt: platinum; PPy: polypyrrole; c-MWCNT: carboxylated multiwalled carbon nanotube; TiO_2: titanium dioxide; ITO: indium tin oxide; poly-TTCA: poly-5,2′:5′,2″-terthiophine-3-carboxylic acid; CV: cyclic voltammetry; and DPV: differential pulse voltammetry.

2.2. Electrochemical Biosensing Response of the XOs/PoPD@g-C_3N_4/ITO Electrode. The electrochemical biosensing response study for the XOs/PoPD@g-C_3N_4/ITO electrode has been carried out by varying Xn concentrations (0.001−1 μM) (Figure 5A). The peak current response increased linearly from 0.001 to 1 μM (Figure 5B), confirming the PoPD@g-C_3N_4 nanocomposite's efficiency and good electrocatalytic capabilities for Xn detection. The sensitivity of the biosensor was calculated to be 5.798 μAM^{-1}, using the regression equation $y = 48.403 \times 10^{-6}x + 5.798 \times 10^{-6}$ (y = peak current and x = concentration of Xn) having $R^2 = 0.9217$. Equation 3 σ/S was used to calculate the limit of detection, which was found to be 0.001 nM, where σ is the standard deviation of the bioelectrode and S is the sensitivity derived from the slope of the calibration curve.

2.3. Validation of the Biosensor with the Real Sample. The developed PoPD@g-C_3N_4 nanocomposite-based sensor has been tested for Xn in the fish meat samples using DPV. An easy method suggested by Watanabe et al. has been used to extract Xn from Rohu (*Labeo rohita*) fish and prepare the Xn solution.[21] The DPV study shows that the peak current steadily increases as the concentration of Xn increases from 0.001 to 1 μM. These results were identical to those of the synthetic Xn samples. Various biosensing characteristics of the synthesized XOs/PoPD@g-C_3N_4-based biosensor were compared with previously reported polymer-based biosensors for Xn detection (Table 1). It was observed that the developed biosensor could detect the presence of Xn in fish meat samples with the lowest LOD.

The suggested biosensor was also used to measure the current response for a time ranging from 0 to 5 days at room temperature to examine the level of xanthine in fish extract while preserved for a certain period of time. The findings also showed an increase in xanthine levels which by day 5 had increased 32 times from day one (Figure S4).

2.4. Shelf Life, Reproducibility, and Specificity. Figure 5C shows the shelf life of the PoPD@g-C_3N_4/ITO electrode, determined using the DPV technique. The DPV response of the five bioelectrodes against Xn with 1 μM was observed weekly to test the stability of the XOs/PoPD@g-C_3N_4/ITO electrode. Also, the result indicates that the biosensor is stable for at least 4 weeks when kept at 4 °C in a dry state, and it merely lost 0.4 μA current when compared to the current response of the initial electrode.

Additionally, five parallel electrodes were prepared to investigate the reproducibility of the developed electrochemical sensor. A relative standard deviation of 5.9% was obtained, indicating excellent reproducibility of the newly developed electrochemical sensor (Figure 5D).

The interference test of the biosensor has been conducted by incubating the XOs/PoPD@g-C_3N_4/ITO electrode with the interfering analytes (ascorbic acid, urea, uric acid, sodium benzoate, and glucose) of various concentrations (10-fold) higher than the concentration of Xn. It has been observed that there was a specific current response for every analyte, proving the selectivity of the biosensor for Xn detection (Figure S5). The specificity test was also conducted, and it has been observed that Xn retained its specificity, even in the mixture of interfering analytes. Additionally, we tested the performance of this biosensor at 10-fold excess concentration for all the analytes.

However, the response profiles to sodium benzoate, ascorbic acid, and glucose were relatively comparable, but the response to urea and uric acid was slightly higher than before. The result, expressed as the tolerance limit, shows a relative error of approximately ±5% in determination of the analyte (Table 2). Therefore, XOs/PoPD@g-C_3N_4/ITO can be a good biosensor for Xn recognition.

Table 2. Table of Tolerance Limit for Foreign Analytes

S. no.	analytes	(change in current response) tolerance limit (%)
1.	ascorbic acid	±0.5
2.	urea	±4.9
3.	uric acid	±4.5
4.	sodium benzoate	±1.3
5.	glucose	±1.9

3. CONCLUSIONS

In the present work, a stable binary PoPD@g-C_3N_4 nanocomposite has been synthesized via a simple oxidative polymerization technique. Various spectroscopic and morphological techniques have been used to validate the successful formation of PoPD@g-C_3N_4. An increase in electron transfer values for the PoPD@g-C_3N_4 electrode compared to bare PoPD and g-C_3N_4 makes it promising to be used for the immobilization of XOs. The fabricated XOs/PoPD@g-C_3N_4/

https://doi.org/10.1021/acsomega.2c06727
ACS Omega 2023, 8, 2328−2336

ITO electrode successfully detected Xn in real fish samples with a detection limit of 0.001 nM (S/N = 3). In addition, the developed biosensing electrode offers suitable sensitivity, a very low detection limit, acceptable stability, reproducibility, and anti-interference characteristics. Consequently, the PoPD@g-C_3N_4 nanocomposite-based biosensor proves to be a viable platform for Xn monitoring.

4. MATERIALS AND METHODS

4.1. Chemicals. Melamine (97.5%) was purchased from Central Drug House, Pvt. Ltd. India, ferric chloride (Anhydrous, 96% $FeCl_3$) was procured from Rankem, India, and 1,2-phenylenediamine (o-PD, 99.5%), glutaraldehyde, xanthine oxidase (XOs, ≥7 units/mg protein), and xanthine (≥99.5%) were purchased from Sigma-Aldrich, USA. Double-distilled water (Milli-Q, Millipore, 18.2 MU) was used to prepare the solutions, and all the glassware was autoclaved before use.

4.2. Synthesis of g-C_3N_4. Melamine was thermally condensed to form graphitic carbon nitride (g-C_3N_4). Typically, 10 g of melamine was added to a crucible with a lid. The crucible was then placed in a muffle furnace and heated for 4 h at a rate of 5 °C min^{-1}, reaching a temperature of 550 °C. The product was collected, crushed into powder, and allowed to cool to room temperature.[47]

4.3. Synthesis of PoPD. The 1,2-phenylenediamine (*o*-PD) monomer (5 g) has been added to a 100 mL conical flask containing ethanol and water 1:1 v/v (25 mL). $FeCl_3$ (4 g) was added to the reaction mixture as an oxidant. The solution changed its color from transparent to brown, indicating rapid polymerization of the monomer. The flask was then subjected to sonication for 2 h, and the temperature was maintained at 30 °C. The synthesized PoPD was removed and repeatedly washed with distilled water/ethanol. To ensure that almost all water and contaminants were completely removed from the material, it was dried for 72 h at 70 °C in a vacuum oven.

4.4. One-Pot Synthesis of the PoPD@g-C_3N_4 Nanohybrid. To prepare the PoPD@g-C_3N_4 nanocomposite, 2.5 g of *o*-phenylenediamine (OPD) was ultrasonicated after being dispersed in 50 mL of DI water. Then, 1.5 g of g-C_3N_4 was added to the mixture, and the solution was ultrasonicated for 30 min. After that, 1.75 g of $FeCl_3$ was added to the mixture and heated at 60 °C for 24 h. The mixture was cooled before being washed with ethanol and DI water. The obtained filtrate was vacuum-dried and heated to 400 °C, forming a light brownish powder.

4.5. Electrophoretic Deposition of the PoPD@g-C_3N_4 Nanocomposite. The PoPD@g-C_3N_4 nanohybrid was deposited electrophoretically onto a hydrolyzed ITO electrode using a two-electrode setup. Both electrodes were positioned 0.5 cm apart. Before deposition, the PoPD@g-C_3N_4 nanohybrid was sonicated in DI water until a clear solution was obtained. For EPD, 10 mL of the solution was diluted with 5 mL of ethanol, and the film was deposited at 12 V for 15 s.

4.6. Fabrication of the PoPD@g-C_3N_4 Nanohybrid-Based Biosensor. For the immobilization of XOs, the PoPD@g-C_3N_4/ITO electrode was incubated with 0.1% glutaraldehyde and left at room temperature for 2 h to activate the functional group on the electrode surface. Afterward, the electrode was washed with phosphate buffer saline (PBS 100 mM, pH 7.4), followed by the covalent immobilization of XOs. The methodology for developing the electrode and synthesizing the PoPD@g-C_3N_4 nanohybrid is shown in Figure 1.

4.7. Instrumentation. The XRD pattern in the 2θ range (10−80°) was recorded using the Bruker D8 ADVANCE X-ray Diffractometer with monochromatic (Cu Kα) radiation (λ = 1.5406 Å), at a scan speed of 2°/min. To investigate the formation of PoPD@g-C_3N_4, FT-IR experiments were carried out using Nicolet TM iS10 in a frequency range of 400−4000 cm^{-1}. The surface morphology of g-C_3N_4/ITO and PoPD@ g-C_3N_4/ITO was studied using FESEM (FEI NOVA NANO-SEM 450). Electrochemical studies were carried out in phosphate buffer (PBS, 100 mM, pH 7.4, 0.9% NaCl) containing 5 mM $[Fe(CN)_6]^{3-/4-}$, using an Autolab potentiostat/galvanostat (Eco-Chemie, Netherlands) with ITO as a working electrode, platinum as an auxiliary electrode, and Ag/AgCl as a reference electrode.

■ ASSOCIATED CONTENT

Supporting Information

The Supporting Information is available free of charge at https://pubs.acs.org/doi/10.1021/acsomega.2c06727.

Fabrication of the PoPD@g-C_3N_4 nanohybrid-based biosensor (PDF)
XRD and FT-IR spectra (PDF)
FESEM images (PDF)
Nyquist diagram and CV studies (PDF)
DPV studies, calibration plot, shelf-life tests, and reproducibility study (PDF)
Scan rate study of the XOs/PoPD@g-C_3N_4/ITO electrode, loading volume optimization of XOs, pH optimization, increase in Xn concentration as a function of days, interference studies, and FESEM images of PoPD@g-C_3N_4/ITO and XOs/PoPD@g-C_3N_4/ITO electrodes (PDF)

■ AUTHOR INFORMATION

Corresponding Authors

Chandra Mouli Pandey − *Department of Chemistry, Faculty of Science, SGT University, Gurugram 122505 Haryana, India;* orcid.org/0000-0003-0079-0586; Email: cmp.npl@gmail.com

Devendra Kumar − *Department of Applied Chemistry, Delhi Technological University, Delhi 110042, India;* orcid.org/0000-0001-9118-2070; Email: dkumar@dce.ac.in

Author

Deeksha Thakur − *Department of Applied Chemistry, Delhi Technological University, Delhi 110042, India;* orcid.org/0000-0003-4205-7139

Complete contact information is available at: https://pubs.acs.org/10.1021/acsomega.2c06727

Notes

The authors declare no competing financial interest.

■ ACKNOWLEDGMENTS

Deeksha acknowledges DST-INSPIRE for the SRF Award. C.M.P. acknowledges the Department of Science and Technology, New Delhi, India, for the DST-INSPIRE Faculty award.

■ REFERENCES

(1) Zhao, Z.; Sun, Y.; Dong, F. Graphitic carbon nitride based nanocomposites: a review. *Nanoscale* **2015**, *7*, 15−37.

(2) Goettmann, F.; Fischer, A.; Antonietti, M.; Thomas, A. Metal-free catalysis of sustainable Friedel−Crafts reactions: direct activation of benzene by carbon nitrides to avoid the use of metal chlorides and halogenated compounds. *J.C.C.* **2006**, *43*, 4530−4532.
(3) Xing, W.; Li, C.; Chen, G.; Han, Z.; Zhou, Y.; Hu, Y.; Meng, Q. Incorporating a novel metal-free interlayer into g-C3N4 framework for efficiency enhanced photocatalytic H2 evolution activity. *Appl. Catal., B* **2017**, *203*, 65−71.
(4) Fahimirad, B.; Asghari, A.; Rajabi, M. Magnetic graphitic carbon nitride nanoparticles covalently modified with an ethylenediamine for dispersive solid-phase extraction of lead(II) and cadmium(II) prior to their quantitation by FAAS. *Microchim. Acta* **2017**, *184*, 3027−3035.
(5) Idris, A.; Oseghe, E.; Msagati, T. A. M.; Kuvarega, A.; Feleni, U.; Mamba, B. Graphitic Carbon Nitride: A Highly Electroactive Nanomaterial for Environmental and Clinical Sensing. *Sensors* **2020**, *20*, 5743.
(6) Zhu, J.; Xiao, P.; Li, H.; Carabineiro, S. A. C. Graphitic Carbon Nitride: Synthesis, Properties, and Applications in Catalysis. *ACS Appl. Mater. Interfaces* **2014**, *6*, 16449−16465.
(7) Xing, W.; Chen, G.; Li, C.; Sun, J.; Han, Z.; Zhou, Y.; Hu, Y.; Meng, Q. Construction of Large-Scale Ultrathin Graphitic Carbon Nitride Nanosheets by a Hydrogen-Bond-Assisted Strategy for Improved Photocatalytic Hydrogen Production and Ciprofloxacin Degradation Activity. *ChemCatChem* **2016**, *8*, 2838−2845.
(8) Chen, X.; Liu, L.; Zhao, Y.; Zhang, J.; Li, D.; Hu, B.; Hai, X. A Novel Metal-Free Polymer-Based POPD/g-C3N4 Photocatalyst with Enhanced Charge Carrier Separation for the Degradation of Tetracycline Hydrochloride. *ChemistrySelect* **2017**, *2*, 9256−9260.
(9) Huo, P.; Lu, Z.; Liu, X.; Wu, D.; Liu, X.; Pan, J.; Gao, X.; Guo, W.; Li, H.; Yan, Y. Preparation photocatalyst of selected photo-degradation antibiotics by molecular imprinting technology onto TiO2/fly-ash cenospheres. *Chem. Eng. J.* **2012**, *189−190*, 75−83.
(10) Huo, P.; Lu, Z.; Liu, X.; Liu, X.; Gao, X.; Pan, J.; Wu, D.; Ying, J.; Li, H.; Yan, Y. Preparation molecular/ions imprinted photo-catalysts of La3+@POPD/TiO2/fly-ash cenospheres: Preferential photodegradation of TCs antibiotics. *Chem. Eng. J.* **2012**, *198−199*, 73−80.
(11) Kirwan, S. M.; Rocchitta, G.; McMahon, C. P.; Craig, J. D.; Killoran, S. J.; O'Brien, K. B.; Serra, P. A.; Lowry, J. P.; O'Neill, R. D. Modifications of Poly(o-phenylenediamine) Permselective Layer on Pt-Ir for Biosensor Application in Neurochemical Monitoring. *Sensors* **2007**, *7*, 420−437.
(12) Kamil Reza, K.; Singh, M. K.; Yadav, S. K.; Singh, J.; Agrawal, V. V.; Malhotra, B. D. Quantum dots based platform for application to fish freshness biosensor. *Sens. Actuators, B* **2013**, *177*, 627−633.
(13) Sahyar, B. Y.; Kaplan, M.; Ozsoz, M.; Celik, E.; Otles, S. Electrochemical xanthine detection by enzymatic method based on Ag doped ZnO nanoparticles by using polypyrrole. *Bioelectrochemistry* **2019**, *130*, 107327.
(14) Devi, R.; Yadav, S.; Pundir, C. S. Electrochemical detection of xanthine in fish meat by xanthine oxidase immobilized on carboxylated multiwalled carbon nanotubes/polyaniline composite film. *Biochem. Eng. J.* **2011**, *58−59*, 148−153.
(15) Albelda, J. A. V.; Uzunoglu, A.; Santos, G. N. C.; Stanciu, L. A. Graphene-titanium dioxide nanocomposite based hypoxanthine sensor for assessment of meat freshness. *Biosens. Bioelectron.* **2017**, *89*, 518−524.
(16) Lawal, A. T.; Adeloju, S. B. Progress and recent advances in fabrication and utilization of hypoxanthine biosensors for meat and fish quality assessment: a review. *Talanta* **2012**, *100*, 217−228.
(17) Jalil, O.; Pandey, C. M.; Kumar, D. Electrochemical biosensor for the epithelial cancer biomarker EpCAM based on reduced graphene oxide modified with nanostructured titanium dioxide. *Microchim. Acta* **2020**, *187*, 275.
(18) Yadav, S. K.; Singh, J.; Agrawal, V. V.; Malhotra, B. D. Nanostructured nickel oxide film for application to fish freshness biosensor. *Appl. Phys. Lett.* **2012**, *101*, 023703.
(19) Solanki, S.; Pandey, C. M.; Gupta, R. K.; Malhotra, B. D. Emerging Trends in Microfluidics Based Devices. *Biotechnol. J.* **2020**, *15*, No. e1900279.
(20) Dolmaci, N.; Çete, S.; Arslan, F.; Yaşar, A. An amperometric biosensor for fish freshness detection from xanthine oxidase immobilized in polypyrrole-polyvinylsulphonate film. *Artif. Cell Blood Substit. Biotechnol.* **2012**, *40*, 275−279.
(21) Thakur, D.; Pandey, C.; Kumar, D. Highly Sensitive Enzymatic Biosensor Based on Polyaniline-Wrapped Titanium Dioxide Nano-hybrid for Fish Freshness Detection. *Appl. Biochem. Biotechnol.* **2022**, *194*, 3765−3778.
(22) Görgülü, M.; Çete, S.; Arslan, H.; Yaşar, A. Preparing a new biosensor for hypoxanthine determination by immobilization of xanthine oxidase and uricase in polypyrrole-polyvinyl sulphonate film. *Artif. Cell Nanomed. Biotechnol.* **2013**, *41*, 327−331.
(23) Erol, E.; Yildirim, E.; Cete, S. Construction of biosensor for hypoxanthine determination by immobilization of xanthine oxidase and uricase in polypyrrole-paratoluenesulfonate film. *J. Solid State Electrochem.* **2020**, *24*, 1695−1707.
(24) Zhang, L.; Lei, J.; Zhang, J.; Ding, L.; Ju, H. Amperometric detection of hypoxanthine and xanthine by enzymatic amplification using a gold nanoparticles−carbon nanohorn hybrid as the carrier. *Analyst* **2012**, *137*, 3126−3131.
(25) Dervisevic, M.; Custiuc, E.; Çevik, E.; Şenel, M. Construction of novel xanthine biosensor by using polymeric mediator/MWCNT nanocomposite layer for fish freshness detection. *Food Chem.* **2015**, *181*, 277−283.
(26) Dervisevic, M.; Custiuc, E.; Çevik, E.; Durmus, Z.; Şenel, M.; Durmus, A. Electrochemical biosensor based on REGO/Fe3O4 bionanocomposite interface for xanthine detection in fish sample. *Food Control* **2015**, *57*, 402−410.
(27) Dervisevic, M.; Dervisevic, E.; Azak, H.; Çevik, E.; Şenel, M.; Yildiz, H. B. Novel amperometric xanthine biosensor based on xanthine oxidase immobilized on electrochemically polymerized 10-[4H-dithieno(3,2-b:2′,3′-d)pyrrole-4-yl]decane-1-amine film. *Sens. Actuators, B* **2016**, *225*, 181−187.
(28) Malhotra, D.; Tran, P. K. L.; Tran, D. T.; Kim, N. H.; Lee, J. H. Cobalt-doped cerium oxide nanocrystals shelled 1D SnO2 structures for highly sensitive and selective xanthine detection in biofluids. *J. Colloid Interface Sci.* **2021**, *600*, 299−309.
(29) Wang, Z.; Liao, F.; Yang, S.; Guo, T. A Novel Route Synthesis of Poly(ortho-phenylenediamine) Fluffy Microspheres Self-assembled from Nanospheres. *Fibers Polym.* **2011**, *12*, 997−1001.
(30) Rashidizadeh, A.; Ghafuri, H.; Esmaili Zand, H. R.; Goodarzi, N. Graphitic Carbon Nitride Nanosheets Covalently Functionalized with Biocompatible Vitamin B1: Synthesis, Characterization, and Its Superior Performance for Synthesis of Quinoxalines. *ACS Omega* **2019**, *4*, 12544−12554.
(31) Cao, J.-L.; Qin, Q.; Wang, Y.; Zhang, H.; Sun, G.; Zhang, Z. Solid-State Method Synthesis of SnO2-Decorated g-C3N4 Nano-composites with Enhanced Gas-Sensing Property to Ethanol. *Materials* **2017**, *10*, 604.
(32) Shcherban, N.; Mäki-Arvela, P.; Aho, A.; Sergiienko, S.; Yaremov, P.; Eränen, K.; Murzin, D. Melamine-derived graphitic carbon nitride as a new effective metal-free catalyst for Knoevenagel condensation of benzaldehyde with ethylcyanoacetate. *Catal. Sci. Technol.* **2018**, *8*, 2928−2937.
(33) Elshafie, M.; Younis, S. A.; Serp, P.; Gad, E. A. M. Preparation characterization and non-isothermal decomposition kinetics of different carbon nitride sheets. *Egypt. J. Pet.* **2020**, *29*, 21−29.
(34) Paulraj, P.; Manikandan, D.; Manikandan, M.; Pandian, P.; Moodley, M.; Roro, K.; Murugan, K. Solid-State Synthesis of POPD@AgNPs Nanocomposites for Electrochemical Sensors. *J. Nanosci. Nanotechnol.* **2018**, *18*, 3991−3999.
(35) Pareek, S.; Quamara, J. Dielectric and optical properties of graphitic carbon nitride−titanium dioxide nanocomposite with enhanced charge sepaeration. *J. Mater. Sci.* **2018**, *53*, 604−612.

https://doi.org/10.1021/acsomega.2c06727
ACS Omega 2023, 8, 2328−2336

(36) Soni, A.; Pandey, C. M.; Pandey, M. K.; Sumana, G. Highly efficient Polyaniline-MoS_2 hybrid nanostructures based biosensor for cancer biomarker detection. *Anal. Chim. Acta* **2019**, *1055*, 26−35.
(37) Abaci, S.; Nessark, B.; Riahi, F. Preparation and characterization of polyaniline+TiO2 composite films. *Ionics* **2014**, *20*, 1693−1702.
(38) Elgrishi, N.; Rountree, K. J.; McCarthy, B. D.; Rountree, E. S.; Eisenhart, T. T.; Dempsey, J. L. A Practical Beginner's Guide to Cyclic Voltammetry. *J. Chem. Educ.* **2018**, *95*, 197−206.
(39) Laviron, E. General expression of the linear potential sweep voltammogram in the case of diffusionless electrochemical systems. *J. Electroanal. Chem. Interfacial Electrochem.* **1979**, *101*, 19−28.
(40) Sen, S.; Sarkar, P. An interference-free new xanthine biosensor based on immobilized enzyme-nanogold conjugate on carbon nanotube doped poly(3,4-Ethylenedioxythiophene) composite film. *Int. J. Biol. Macromol.* **2022**, *199*, 275−286.
(41) Joon, A.; Ahlawat, J.; Aggarwal, V.; Jaiwal, R.; Pundir, C. S. An improved amperometric determination of xanthine with xanthine oxidase nanoparticles for testing of fish meat freshness. *Sens. Bio-Sens. Res.* **2021**, *33*, 100437.
(42) Yazdanparast, S.; Benvidi, A.; Abbasi, S.; Rezaeinasab, M. Enzyme-based ultrasensitive electrochemical biosensor using poly(l-aspartic acid)/MWCNT bio-nanocomposite for xanthine detection: A meat freshness marker. *Microchem. J.* **2019**, *149*, 104000.
(43) Devi, R.; Yadav, S.; Pundir, C. S. Amperometric determination of xanthine in fish meat by zinc oxide nanoparticle/chitosan/multiwalled carbon nanotube/polyaniline composite film bound xanthine oxidase. *Analyst* **2012**, *137*, 754−759.
(44) Devi, R.; Yadav, S.; Pundir, C. S. Au-colloids−polypyrrole nanocomposite film based xanthine biosensor. *Colloids Surf., A* **2012**, *394*, 38−45.
(45) Dervisevic, M.; Dervisevic, E.; Çevik, E.; Şenel, M. Novel electrochemical xanthine biosensor based on chitosan−polypyrrole−gold nanoparticles hybrid bio-nanocomposite platform. *J. Food Drug Anal.* **2017**, *25*, 510−519.
(46) Rahman, M. A.; Won, M.-S.; Shim, Y.-B. Xanthine Sensors Based on Anodic and Cathodic Detection of Enzymatically Generated Hydrogen Peroxide. *Electroanalysis* **2007**, *19*, 631−637.
(47) Rajkumar, C.; Kim, H. Hybrid nanostructures of Pd−WO3 grown on graphitic carbon nitride for trace level electrochemical detection of paraoxon-ethyl. *Microchim. Acta* **2021**, *188*, 233.

https://doi.org/10.1021/acsomega.2c06727
ACS Omega 2023, 8, 2328−2336